Journal of Polymers and the Environment (2020) 28:995–1009
https://doi.org/10.1007/s10924-020-01664-4

ORIGINAL PAPER

# Amidoxime Modified Polymers of Intrinsic Microporosity (PIM-1); A Versatile Adsorbent for Efficient Removal of Charged Dyes; Equilibrium, Kinetic and Thermodynamic Studies

**Bekir Satilmis**[1]

Published online: 27 January 2020


## Abstract

Polymers of Intrinsic Microporosity (PIMs) are recognized as promising polymers for active separation of organic pollutants. These highly porous and solution-processable polymers could be tailored to remove specific targets from an aqueous system. In this study, PIM-1 powder was modified to amidoxime PIM-1 powder and adsorption of charged dyes which are Methylene Blue (MB, cationic) and Methyl Orange (MO, anionic) from an aqueous system was explored to evaluate the influence of contact time, initial concentration, solution pH and temperature on the removal of dyes. The adsorption reached the equilibrium within three hours in a batch adsorption process for both dyes. Experimental adsorption capacity ($q_{e,\,exp}$) of Amidoxime PIM-1 was found as 79.8 mg $g^{-1}$ and 69.8 mg $g^{-1}$ for MO and MB, respectively at pH 6 and 298 K. The Amidoxime PIM-1 was also able to remove a mixture of anionic and cationic dyes simultaneously from aqueous system. The removal ability is dependent on the solution pH and the selectivity can be tuned by shifting solution pH such as at low pH (pH 3) anionic dye adsorption is more favourable, while at high pH (pH 10) cationic dye adsorption is preferable. Equilibrium data acquired from batch adsorption experiments have been examined by four two-parameter (Langmuir, Freundlich, Temkin and Dubinin–Radushkevich), four three-parameter (Redlich–Peterson, Sips, Khan and Liu) isotherm models, and by kinetic models such as the pseudo-first-order, the pseudo-second-order, Elovich equation and intraparticle diffusion using non-linear regression technique. Combination of several errors analysis techniques was applied to find the best fitting isotherm and kinetic models. Liu isotherm was the best to define the experimental data and the maximum adsorption capacities ($q_m$) were calculated as 86.7 mg $g^{-1}$ and 81.3 mg $g^{-1}$ for MO and MB, respectively at pH 6 and 298 K. Adsorption data have the best consistency with the pseudo-second-order kinetic model. Furthermore, thermodynamic parameters were determined and the experiments suggested that the adsorption of MB and MO onto Amidoxime PIM-1 is a physical, spontaneous and exothermic.

**Electronic supplementary material** The online version of this article (https://doi.org/10.1007/s10924-020-01664-4) contains supplementary material, which is available to authorized users.

✉ Bekir Satilmis
bekir.satilmis@ahievran.edu.tr

[1] Department of Medical Services and Techniques, Vocational School of Health Services, Kirsehir Ahi Evran University, 40100 Kirsehir, Turkey

**Graphic Abstract**

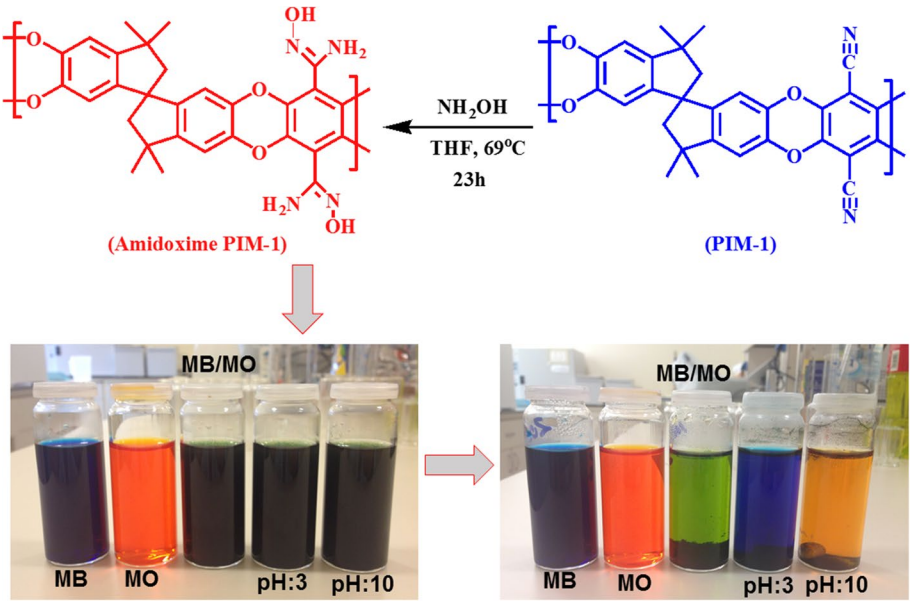


**Keywords** Polymers of intrinsic microporosity (PIMs) · Adsorption · Isotherm · Kinetic · Thermodynamic · Methylene Blue · Methyl Orange

## Introduction

Industrial operations of organic dyes have been increased in parallel with population growth and technological developments [1, 2]. A wide range of industries utilizes dyes to make their products appealing. However, the excessive use of these dyes also poses a threat to human health and environment as they are mostly emitted into the environment without using appropriate discharging method [3]. Therefore, effective removal of dyes from water is an indispensable and an urgent issue for environmental remediation. Therefore, new materials have been developed to alleviate this problem including polymers [4, 5], composites [6, 7], agriculture wastes [8, 9] and microorganisms [10, 11] etc. Furthermore, various techniques have been adapted for dye removal including adsorption, membrane separation [12], biodegradation [13], coagulation [14] and oxidation and extraction [15]. However, most of these techniques are expensive and require sludge disposal. Thus, adsorption is considered a more promising method for dye removal since it does not require complex systems for dye removal [16–20].

Polymers of Intrinsic Microporosity (PIMs) have a rigid and contorted structure which provides a permanent porosity to the PIM polymers. They exhibit high free-volume which makes them desirable for adsorption and separation applications [21–23]. PIM-1 is the first synthesised polymer of this family, which could be produced by a one-pot polycondensation reaction using commercially available spirobisindane and tetrafluoroterephthalonitrile monomers. High surface area and the solubility in common organic solvents such as tetrahydrofuran and chloroform enable a wide spectrum of application opportunities to PIM-1 in various forms including powder [23], film [24] and fiber [25] forms. All of them have been successfully used for organic removals from water [23–28]. Even though PIM-1 has a specific affinity for a neutral species, the adsorption ability could be tailored for the desired species by modifying the nitrile group in polymer backbone [23]. Accordingly, hydrolyzed PIM-1s demonstrate a high affinity for cationic molecules and they can remove cationic species from an aqueous system depend on the degree of hydrolysis/carboxylation [29]. On the other hand, amine, ethanolamine and di-ethanolamine modified PIM-1s exhibit high affinity for anionic molecules and they can selectively remove anionic molecules from water [23]. Recently, we have reported the efficient removal of dyes by modified PIM-1s in the form of powder [29, 30] and fibrous membranes [31, 32]. Fibrous membranes could be prepared by electrospinning technique [33, 34], which provide more practical uses for modified PIM-1s. Moreover, modified PIM-1s were also used for metal-ion removal. Especially, amidoxime modified PIM-1 could be employed in uranium separation from water since amidoxime functionality has the chelating ability with uranyl ions [35–37]. Although previously studied hydrolyzed and

amine modified PIM-1s show selective separation efficiency, which could be favourable for some operations such as the recovery of bio-refinery products [38] and isolation of natural products [39], when it comes to practical dye removal, versatile materials could be more promising.

Therefore, in this research, we have first synthesised amidoxime PIM-1 and then, the dye removal efficiency of amidoxime PIM-1 was evaluated using cationic (Methylene Blue) and anionic (Methyl Orange) dyes from water. To the best of our knowledge, no report has been published considering the dye removal efficiency of amidoxime PIM-1. As we envisaged, it can remove both cationic and anionic dyes from an aqueous system effectively. With the affinity against both cationic and anionic species, amidoxime PIM-1 could be a promising material for various separation applications since it can be produced in the form of dense and fibrous membranes which provide significant practical use in removal applications. Moreover, the uptake ability of amidoxime PIM-1 could be tuned for desired species by adjusting the pH, unlike other modified PIMs. Furthermore, the parameters affecting the adsorption capacity including the contact time, temperature, and the dye concentration were examined. Consequently, equilibrium isotherms, kinetic models and thermodynamic parameters were determined.

## Experimental

### Materials

Anhydrous Potassium carbonate (99.0%), 5,5′,6,6′-Tetrahydroxy-3,3,3′,3′-tetramethyl-1,1′-spirobisindane (98%), and tetrafluoroterephthalonitrile (98%) were purchased from Alfa Aeser and they were purified as reported in our previous study [32]. Hydroxylamine (50% in $H_2O$), ethanol (EtOH, ≥ 99.8%), dimethylacetamide (DMAc, ≥ 99.5%), tetrahydrofuran (THF, ≥ 99.9%), toluene (≥ 99.5%) and anhydrous Methylene Blue ($C_{16}H_{18}ClN_3S{\cdot}xH_2O$; molecular weight: 319.85) were obtained from Sigma Aldrich and were used as received. Methyl Orange ($C_{14}H_{14}N_3NaO_3S$; molecular weight: 327.3) was purchased from Merck and was used as received.

### Synthesis and Characterization of PIM-1 and Amidoxime Modified PIM-1

Synthesis and characterization of PIM-1 powder was performed in our previous study [40]. Briefly, PIM-1 was prepared using 5,5′,6,6′-Tetrahydroxy-3,3,3′,3′-tetramethyl-1,1′-spirobisindane (TTSBI) and tetrafluoroterephthalonitrile (TFTN) as monomers in the presence of potassium carbonate catalyst in dimethylacetamide-toluene mixture at 160 °C. Likewise, amidoxime PIM-1 powder was synthesized and characterized similar to our previous report [35]. Complete dissolution of PIM-1 powder was achieved in THF and an appropriate amount of hydroxylamine was added slowly to this solution which was kept stirring at 69 °C for 23 h under reflux. Transparent solution was precipitated in ethanol to obtain off-white product.

### Methods

Bruker Vertex 70 FTIR spectroscopy was utilized to record FTIR spectra of samples in the attenuated total reflection (ATR) mode using a resolution of 4 $cm^{-1}$ and 64 scans. $^1H$ NMR experiments were performed in Bruker DPX-400 MHz using $CDCl_3$ and $d_6$-DMSO as solvents. Thermal changes of the samples were monitored by TA Q500 thermogravimetric analyzer. The samples were dried at 120 °C before analysis to remove residual and then heated at 20 °C $min^{-1}$ under $N_2$ atmosphere. $N_2$ adsorption experiments were performed on a Quantachrome Autosorb iQ apparatus at 77 K. Samples were degassed for at least 12 h at 120 °C prior to analysis. Elemental analysis of the samples was determined using Thermo Scientific Flash 2000 series CHNS-O analyzer and X-ray photoelectron spectroscopy (XPS, Thermo Fisher Scientific K-Alpha XPS Spectrometer). Absorbance of the dye solutions were determined using Genesis10s UV visible spectrometer.

### Sorption Studies

Dye adsorption ability of amidoxime PIM-1 powder was evaluated using charged dyes namely Methylene Blue (MB, cationic dye) and Methyl Orange (MO, anionic dye) in deionized water. Absorbance values of the calibration solutions were recorded using a Genesis 10 s UV–Visible spectrometer at $\lambda_{max}$ values of 664 and 464 nm for MB and MO, respectively. Dry amidoxime PIM-1 powder (~ 10.0 mg) was placed in 20 mL of 40–500 mg $L^{-1}$ dye solutions. The dye solution (~ pH: 6) containing the amidoxime PIM-1 was stirred well for 3 h. 100 µL aliquots were taken by pipette and diluted by certain amount of deionized water. The amount of dye adsorbed by the polymer, $qe$ (mg $g^{-1}$), was determined from the Eq. 1

$$q_e = \frac{(C_0 - C_e) \times V}{w} \tag{1}$$

where $C_0$ (mg $L^{-1}$), $C_e$ (mg $L^{-1}$), V (L) and w (g) represent initial concentration of dye, concentration of dye at equilibrium; volume of dye solution; and amount of amidoxime PIM-1, respectively.

The impact of contact time was examined using 100 mg $L^{-1}$ dye solutions for a period of 8 h. The influence of initial dye concentration on the adsorption capacity of amidoxime

PIM-1 powder was conducted at 40, 50, 100, 200, 350 and 500 mg $L^{-1}$ concentrations at natural pH (pH 6). The influence of temperature on the adsorption ability of amidoxime PIM-1 was studied using the solution temperatures of 283, 298, 313 K for the same dye concentrations (40–500 mg $L^{-1}$). The effect of pH on the adsorption was studied by adjusting pH of the dye solutions to 3.0, 6.0 and 10.0 with the help of 1 M NaOH and 1 M HCl at 100 and 500 mg $L^{-1}$ dye concentrations.

Afterwards, adsorption isotherms, kinetic models and thermodynamic parameters were identified. The parameters of adsorption isotherms and kinetic models were determined by non-linear regression analysis method instead of using linear regression analysis. As expressed recently [41], the non-linear method is necessary to obtain correct parameters, especially for thermodynamic parameters. Therefore, solver add-in function of the Microsoft Excel has been used to solve equations by minimizing the sum of error squared (SSE) between the calculated values and the experimental data. The agreement between experimental and calculated data was also quantified using the correlation coefficient ($R^2$), chi-square test ($\chi^2$) and the relative error ($\Delta q$) methods as shown in Eqs. 2–5 [42, 43].

$$SSE = \sum_{i=1}^{n} (q_{e,cal} - q_{e,exp})_i^2 \tag{2}$$

$$R^2 = \frac{(q_{e,exp} - \overline{q}_{e,cal})^2}{\sum (q_{e,exp} - \overline{q}_{e,cal})^2 + (q_{e,exp} - q_{e,cal})^2} \tag{3}$$

$$\chi^2 = \sum_{i=1}^{n} \frac{(q_{e,cal} - q_{e,exp})^2}{q_{e,exp}} \tag{4}$$

$$\Delta q(\%) = \sqrt{\sum \frac{[(q_{e,exp} - q_{e,cal})/q_{e,exp}]^2}{N-1}} \times 100 \tag{5}$$

where ($q_{e,\,exp}$), ($q_{e,\,cal}$), ($\overline{q}_{e,cal}$) are experimental equilibrium capacity, calculated equilibrium capacity and the mean of calculated equilibrium capacity, respectively and N represents the number of the measurements.

## Results and Discussion

### Synthesis and Characterization of PIM-1 and Amidoxime PIM-1

PIM-1 exhibits high surface area (~ 760 $m^2\ g^{-1}$) and high free volume, thus, it has been used extensively for various operations including gas separation, adsorption, sensor and catalysis due to unusual structural properties [44–51]. Figure 1a shows the synthesis of PIM-1 by using commercially available 5,5′,6,6′-Tetrahydroxy-3,3,3′,3′-tetramethyl-1,1′-spirobisindane (TTSBI) and tetrafluoroterephthalonitrile (TFTN) monomers in equimolar quantities by step-growth polymerization. It was previously revealed that parent PIM-1 polymer has high affinity to neutral species in ethanolic solution [23, 24]. On the other hand, it shows almost no affinity against charged species in an aqueous system [23]. This feature could be tailored by an appropriate modification and the adsorption ability can be enhanced for specific targets as reported in our previous studies [23, 29, 30]. While the selectivity against anionic species can be enhanced by amine, ethanolamine and di-ethanolamine modifications, reverse selectivity can be obtained by simple hydrolysis reaction for cationic species [23]. Moreover, these materials could be produced in the dense and the fibrous membrane forms which significantly enhance their use in practical applications [31, 32].

Recently, amidoxime PIM-1 (Fig. 1a), has been reported by Patel et al. [37] which was subsequently used for the removal of uranium from seawater by Shin et al. [36] due to the affinity of amidoxime groups against uranyl ions. Amidoxime PIM-1 shows a decent solubility in dimethylformamide (DMF), thus, we have reported the preparation of amidoxime modified PIM-1 fibrous membrane (FM) [35]. Consequently, amidoxime PIM-1 FM has been employed successfully in a column adsorption study to remove uranyl ions from water to illustrate the practical use of the polymer. While chemical modification of PIM-1 empowers the affinity for specific organic molecules, it usually leads to a considerable reduction in the surface area [29–31]. Also, the resulting polymer may become insoluble that may limit the further use of the modified PIM-1s [30]. The main advantage of amidoxime PIM-1 among other modified PIM-1s is that while it maintains solubility in common organic solvents. It has also remained surface area after modification (~ 550 $m^2\ g^{-1}$) [35]. Although other modified PIM-1s have been studied for dye separation studies from an aqueous system, no one, to the best of our knowledge, has evaluated the dye adsorption ability of amidoxime modified PIM-1 yet. Therefore, we have first reacted PIM-1 with hydroxylamine to obtain amidoxime PIM-1 (Fig. 1a). Then, the characterization of amidoxime PIM-1 was performed according to the reported procedure [35] using FT-IR and $^1$H NMR spectroscopies.

FT-IR spectra of PIM-1 and amidoxime PIM-1 are shown in Fig. 1b which clearly indicates that the typical nitrile stretches (2240 $cm^{-1}$) of PIM-1 is disappeared by modification. Simultaneously, the appearance of C=N (1656 $cm^{-1}$) and N–O (914 $cm^{-1}$) bands along with N–H and O–H stretches (3450–3100 $cm^{-1}$) confirm the successful modification of PIM-1 to amidoxime PIM-1. In addition,

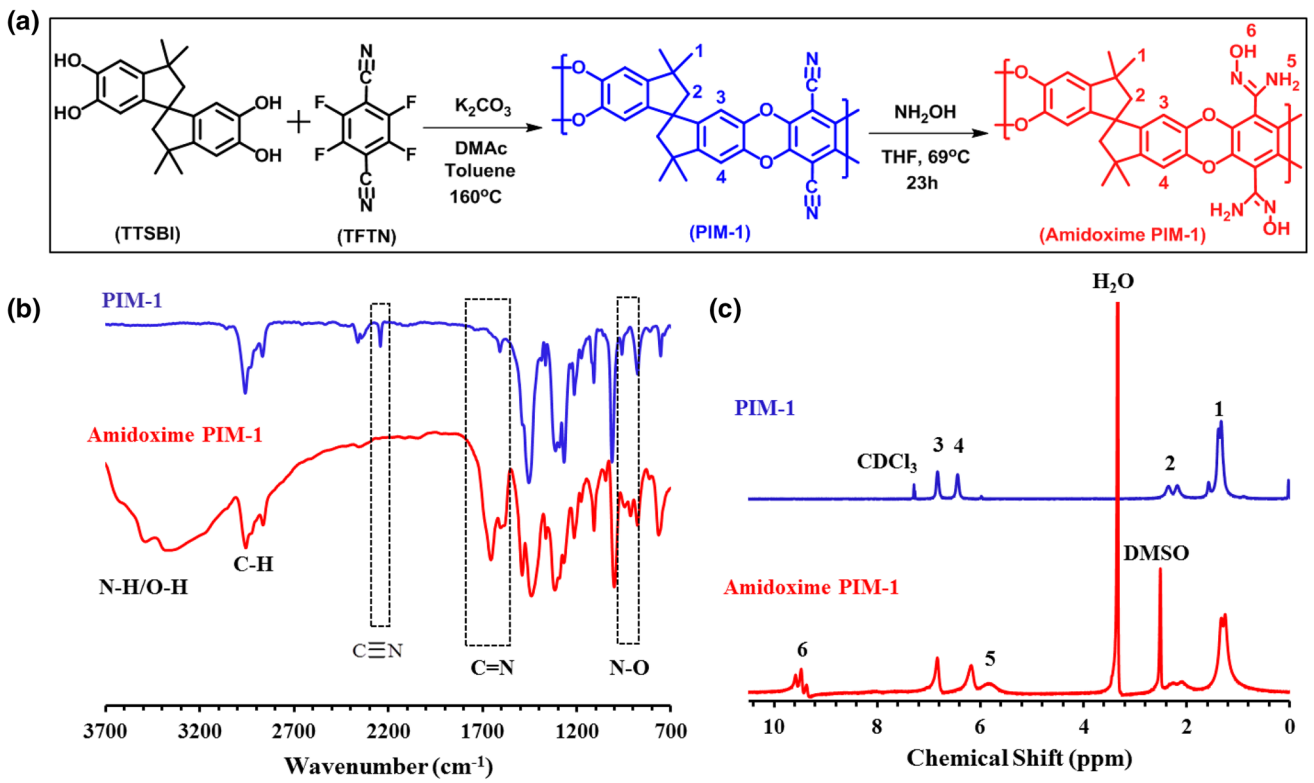


**Fig. 1** **a** Synthesis path of PIM-1 and amidoxime PIM-1, **b** FT-IR and **c** $^{1}$H NMR spectra of PIM-1 and amidoxime PIM-1

the emergence of –$NH_2$ (5.81 ppm) and –OH (9.44 ppm) peaks in $^{1}$H NMR spectra shows the transformation of nitrile to amidoxime as displayed in Fig. 1c [35]. Further characterization data including TGA, XPS, elemental analysis and BET are provided in Fig. S1–S3 and Table S1 in supporting information for PIM-1 and amidoxime PIM-1 samples. Following that we have investigated the affinity of amidoxime PIM-1 against charged dyes using Methylene Blue (MB) and Methyl Orange (MO) as model compounds in a batch adsorption process and the parameters affecting the adsorption were studied.

## The Effect of Contact Time

Initial studies have focussed on determination of adsorption characteristics of amidoxime PIM-1 for MB and MO dyes as a function of time at 100 mg $L^{-1}$ dye concentrations for a period of 8 h (Fig. 2a and b). As is shown in Fig. 2a and b, the adsorption capacities of both dyes are increased rapidly, and more than 50% of adsorption took place during the first 30 min. Then gradually reached the equilibrium within 180 min. The dye uptake remained almost constant after that point. The rapid adsorption at the beginning could be elucidated by the number of vacant sites on the amidoxime PIM-1 and the availability of these vacant sites reduced by the time. Similar behaviour was observed by the various adsorbents [52–54]. Additionally, although the equilibrium time is almost the same for both dyes, the uptake of MO was greater than the uptake of MB throughout the experiment showing amidoxime PIM-1 has a slightly higher affinity for MO compared to MB.

## The Effect of Initial Concentration

The adsorption capacity firmly depends on the initial concentration of the dyes and the available sites on the amidoxime PIM-1 surface. The impacts of initial dye concentrations on the adsorption are illustrated in Fig. 2c for MB and MO, respectively at three different temperatures 283, 298 and 313 K. As can be seen in Fig. 2c, while the adsorption capacity of amidoxime PIM-1 was 30.7 mg $g^{-1}$ at 50 mg $L^{-1}$ MB concentration, the capacity was increased to 69.8 mg $g^{-1}$ at the concentration of 500 mg $L^{-1}$ at 298 K. Similar trend was also monitored for MO adsorption capacity which was increased from 32 to 79.8 mg $g^{-1}$ for the aforementioned concentrations, respectively at 298 K (Fig. 2c). The same tendency was observed when the adsorption is performed at 283 K and 313 K for both MB and MO adsorptions.

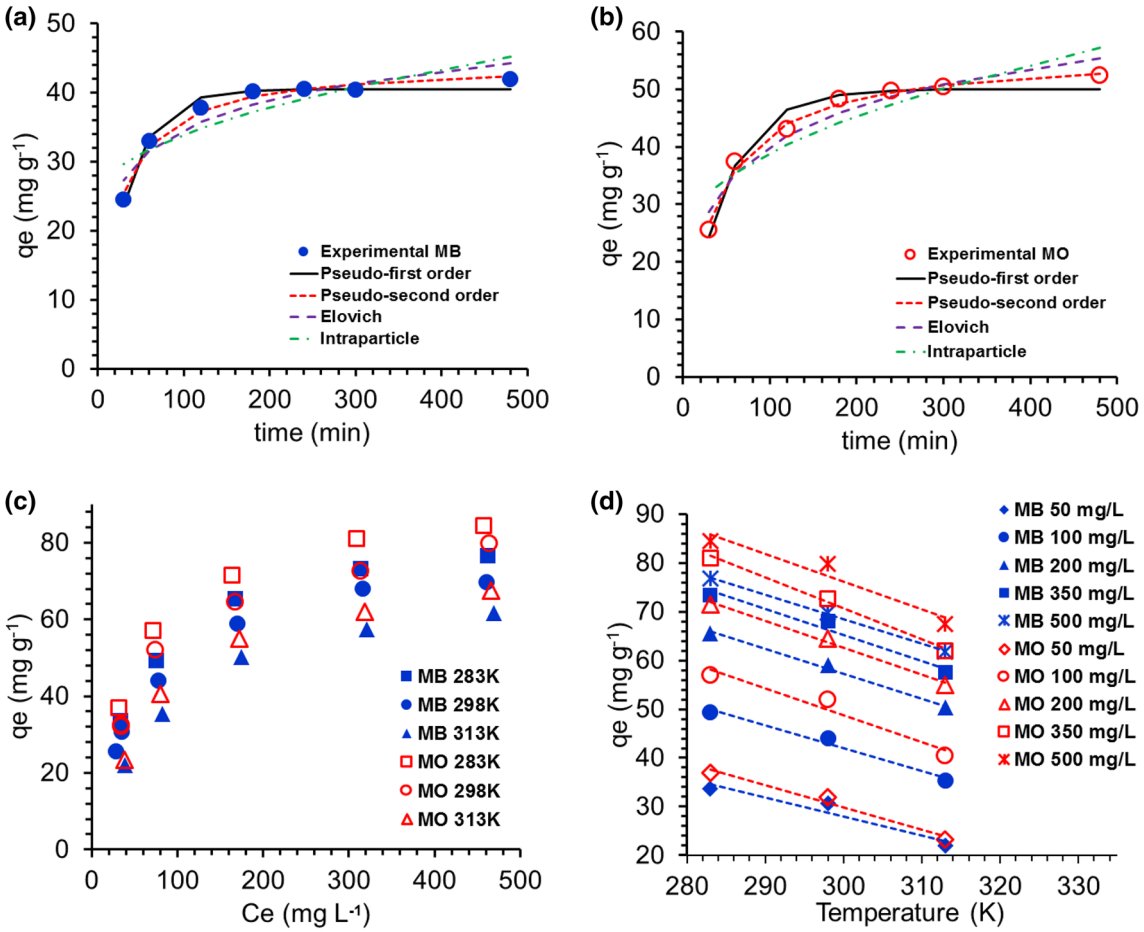


**Fig. 2** Influence of contact time on the adsorption of MB and MO and applied kinetic adsorption models for **a** MB and **b** MO (experiment conditions; 20 mL 100 mg $L^{-1}$ dye solutions, 10 mg of Amidoxime PIM-1, temperature 298 K, pH ~ 6), **c** influence of initial concentration (experiment conditions; 10 mg of Amidoxime PIM-1, pH ~ 6), **d** influence of temperature on the adsorption of MB (filled circles) and MO (open circles) on amidoxime PIM-1 (experiment conditions; 10 mg of Amidoxime PIM-1, pH ~ 6, various dye concentrations)

## The Influence of Temperature

The impact of temperature on the adsorption of MB and MO was examined using three different temperatures (283, 298 and 313 K). Figure 2d displays the equilibrium adsorption capacities against solution temperatures for the adsorption of MB and MO at various concentrations. As displayed, temperature has a negative impact on the adsorption of both dyes. The equilibrium adsorption capacity reduced from 76.8 to 61.7 mg $g^{-1}$ for MB and from 84.4 to 67.4 mg $g^{-1}$ for MO when the solution temperature was raised from 283 to 313 K.

## The Effect of pH and the Adsorption from the Mixture

Amidoxime PIM-1 can remove both MB and MO simultaneously from an aqueous system. To illustrate this, MB/MO mixture solution (5 mL, 10 mg $L^{-1}$ for each dye) was prepared and treated with amidoxime PIM-1 which clears the solution immediately as demonstrated in Fig. S4 in supporting information. Although amidoxime PIM-1 shows a similar affinity for MB and MO, the affinity could easily be tuned by shifting the pH for desired species. While it shows selective and enhanced adsorption for MO at low pH (pH 3), the selectivity could be reversed for MB at pH 10 revealing the versatility of the amidoxime PIM-1 in adsorption applications from water. The influence of pH was investigated using 3 different pH values; 3.0, 6.0 and 10.0. Figure 3a and b display the visual representation of MB and MO solutions before and after in contact with amidoxime PIM-1 at different pH values at 100 mg $L^{-1}$ dye concentrations. As displayed in Fig. 3a, MB solution was completely cleared at pH 10, similarly, MO solution was cleared at pH 3 (Fig. 3b). The maximum adsorption ability of amidoxime PIM-1 at different pH values was studied using 500 mg $L^{-1}$

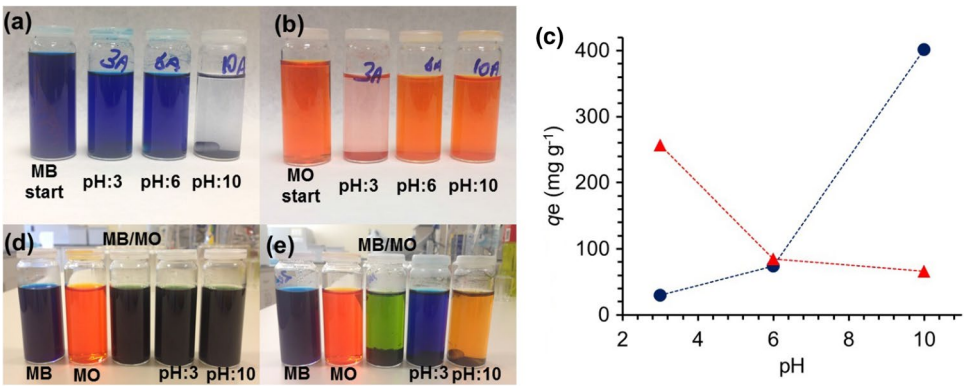


**Fig. 3** Digital images of **a** MB and **b** MO solutions before and after in contact with amidoxime PIM-1 at different pH values (100 mg $L^{-1}$). **c** Relationship between equilibrium adsorption capacities and solution pH for MB (filled circle) and MO (filled triangle) (500 mg $L^{-1}$). Digital images of MB, MO and MB/MO mixture solutions before (**d**) and after (**e**) in contact with amidoxime PIM-1 at pH 3 and 10 (200 mg $L^{-1}$ total dye concentration)

dye solutions and the results are displayed in Fig. 3c. The maximum uptake of MB was found 29.3 mg $g^{-1}$ at pH 3, while the maximum uptake was 401.6 mg $g^{-1}$ at pH 10 for the same dye. Likewise, the adsorption maximum of MO was found 257.3 mg $g^{-1}$ at pH 3, whereas the maximum uptake was 66.4 mg $g^{-1}$ at pH 10, indicating the pH dependence of the adsorption. The pH-dependent selectivity could be further revealed by using binary mixtures of MB and MO. Figure 3d exhibits the digital images of MB and MO solutions and MB/MO mixture solutions before in contact with amidoxime PIM-1. As can be seen, MB/MO mixture is a dark green solution at the beginning, which was precipitated after a certain period due to the opposite charges of MB and MO molecules (Fig. 3e, green solution). When the mixture solution was treated with amidoxime PIM-1 at different pH values, one dye could be cleared selectivity from the mixture solutions (Fig. 3e).

Since amidoxime PIM-1 shows an affinity for both MB and MO dyes, the interactions between dyes and amidoxime PIM-1 in the adsorption process was further studied using the FT-IR technique. Figure 4 displays FT-IR spectra of amidoxime PIM-1 sample before in contact with dye, and amidoxime PIM-1 samples after in contact with MB and MO dyes. As can be seen, no significant shift occurred in amidoxime PIM-1 vibrations only a slight change in the intensity of C=N stretches could be monitored. This reveals that there is no discernible chemical-bond formation occurred between dye molecules and amidoxime PIM-1. Dye molecules and amidoxime PIM-1 has mainly electrostatic interactions.

## Adsorption Kinetics

Determination of kinetic parameters is important in the adsorption since it provides valuable information on the rate of adsorption. Figure 2a and b exhibit the change in

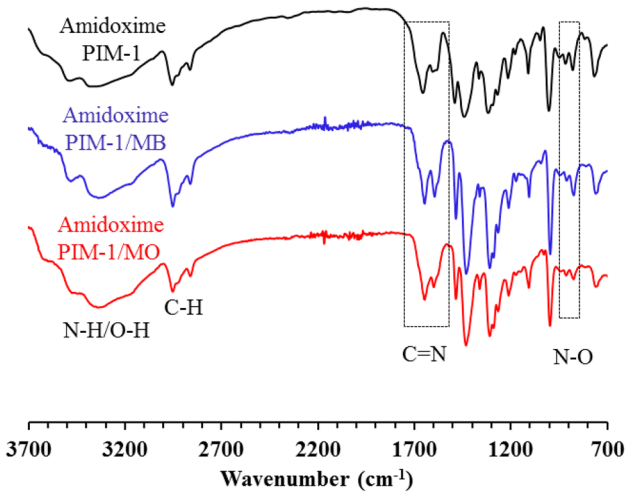


**Fig. 4** FT-IR spectra of untreated amidoxime PIM-1, MB adsorbed amidoxime PIM-1 and MO adsorbed amidoxime PIM-1

equilibrium adsorption ($q_e$) as a function of time. In order to study the adsorption kinetics of MB and MO by Amidoxime PIM-1. The pseudo-first-order [55], pseudo-second-order [56], Elovich equation [57] and intra-particle diffusion [58] were tested by non-linear regression analysis. The non-linear forms of the equations for the applied kinetic models are displayed in Table 1.

Considering kinetic models, the pseudo-first-order kinetic model is more appropriate to define the dynamics of the initial stage. If the process describes by the pseudo-first-order kinetic model, it implies that one dye molecule adsorbs by the one active site of the adsorbent and they usually have weak interactions [59, 60]. On the other hand, if the experimental data follows the pseudo-second-order model, it is suggested that one dye molecule is adsorbed onto two active sites of the adsorbent. In addition, Elovich equation

**Table 1** Equations of kinetic models and comparison of kinetic parameters for MB and MO adsorption on amidoxime PIM-1

| Kinetic model | Equation* | Parameter | Methylene Blue | Methyl Orange |
|---|---|---|---|---|
| | | $q_{e,\,exp.}$(mg $g^{-1}$) | 42.0 | 52.5 |
| Pseudo First Order Model | $q_t = q_{e,cal}(1 - \exp(-k_1 t)$ | $k_1$ ($min^{-1}$) | 0.029 | 0.022 |
| | | $q_{e\,cal}$ (mg $g^{-1}$) | 40.5 | 50.0 |
| | | SSE | 5.3 | 21.0 |
| | | $R^2$ | 0.977 | 0.963 |
| | | $\chi^2$ | 0.15 | 0.49 |
| | | Δq (%) | 2.6 | 4.5 |
| Pseudo Second Order Model | $q_t = \frac{q_{e,cal}^2 k_2 t}{1+q_{e,cal} k_2 t}$ | $k_2$ (g $mg^{-1}$ $min^{-1}$) | 0.0010 | 0.0005 |
| | | $q_{e\,cal}$ (mg $g^{-1}$) | 44.3 | 56.4 |
| | | SSE | 3.1 | 4.6 |
| | | $R^2$ | 0.9997 | 0.9997 |
| | | $\chi^2$ | 0.09 | 0.12 |
| | | Δq (%) | 2.2 | 2.4 |
| Elovich | $q_t = \frac{1}{b} lnab + \frac{1}{b} lnt$ | b (g $mg^{-1}$) | 0.164 | 0.104 |
| | | α (mg $g^{-1}$ $min^{-1}$) | 17.81 | 6.25 |
| | | SSE | 24.5 | 30.2 |
| | | $R^2$ | 0.904 | 0.948 |
| | | $\chi^2$ | 0.75 | 0.82 |
| | | Δq (%) | 6.3 | 6.4 |
| Intraparticle | $q_t = k_i \sqrt{t} + C$ | $k_i$ (mg $g^{-1}$ $min^{-1/2}$) | 0.95 | 1.53 |
| | | C | 24.4 | 23.6 |
| | | SSE | 58.8 | 96.9 |
| | | $R^2$ | 0.994 | 0.993 |
| | | $\chi^2$ | 1.89 | 2.79 |
| | | Δq (%) | 10.4 | 12.1 |

*$q_{e,\,exp}$, $q_{e,\,cal}$ are experimental and calculated equilibrium adsorption capacities, respectively. qt (mg $g^{-1}$) is the adsorption capacity at time *t*. $k_1$, $k_2$, and $k_i$ are the rate constants for the respective equations. α and b are the initial adsorption rate constant and desorption constant of the Elovich model, respectively

is commonly applied to chemisorption kinetics and it is usually valid for systems that contain heterogenous adsorbing surface [57]. The intraparticle diffusion model is used to determine diffusion mechanism and it shows that sorption is a multi-step process in which the sorbate molecules transport from bulk to the external surface of the adsorbent and then moves into internal pores [58, 59]. By plotting $q_t$ versus $t^{0.5}$, a multi-linear graph is observed for MB and MO adsorption on amidoxime PIM-1 as shown in Fig. S5 in supporting information which indicates that more than one step occurs in the adsorption process. As the lines produced by plotting $q_t$ versus *t* do not pass the origin, it could be assumed that be the rate-limiting step was governed by both film diffusion and intraparticle diffusion.

Obtained kinetic parameters from non-linear fittings and their statistical analysis data are presented in Table 1. As suggested by Lima et al. [61], comparing the fitness of kinetic data by using only one error analysis method such as SSE, $R^2$, $\chi^2$ or Δq (%) may mislead the data interpretation. Therefore, using a combination of these analyses would help to distinguish the best kinetic model for the adsorption. For the data presented in Fig. 2a and b, the pseudo-second-order model showed the highest $R^2$ and the lowest SSE, $\chi^2$ and Δq values, indicating the best-fitted model for the adsorption of MB and MO on amidoxime PIM-1. This was followed by pseudo-first-order kinetic model. Based on the error analysis, the lowest degree of fitness was obtained for the Elovich model. Regarding the data obtained from intraparticle diffusion kinetic, the adsorption is a multi-step process in which the rate depends on both film diffusion and intraparticle diffusion [62].

## Adsorption Isotherms

Adsorption isotherms are critical for the estimation of the adsorption mechanism [63]. Therefore, the equilibrium data were defined by two-parameter isotherm models (Langmuir [64], Freundlich [65], Temkin [66] and Dubinin–Radushkevich (D–R) [67]) and three-parameter isotherm models (Redlich–Peterson [68], Sips [69], Khan [70] and Liu [71])

using non-linear regression analysis method. The isotherm equations, isotherm constants and their statistical analysis data are illustrated in Tables 2 and 3 for two and three-parameter isotherm models, respectively. Experimental and calculated adsorption capacities of MB and MO by amidoxime PIM-1 are also compared in Fig. 5 for three different temperatures; 283 K, 298 K, 313 K.

Regarding two-parameter isotherm models, while Langmuir isotherm considers monolayer coverage on the homogenous surface, Freundlich isotherm shows the heterogeneity on the adsorbate surface [42]. Additionally, Temkin isotherm is depended on an empirical equation which is defined based on chemical adsorption. Temkin model considers the effects of adsorbent-adsorbate interactions and infers that the sorption energy would reduce linearly with surface coverage [72]. Furthermore, Dubinin–Radushkevich isotherm is an empirical model where adsorption process follows a pore-filling mechanism. It could be applied to define the adsorption process takes place onto both homogeneous and heterogeneous surfaces [73]. Moreover, the mean free energy ($E = 1/(\sqrt{2K_{DR}})$) can be calculated using isotherm constant ($K_{DR}$). Hence, the mechanism of adsorption can be deduced from the value of E. Correct determination of "E" relies on the units of $K_{DR}$ and Polanyi potential (ε) used in D–R equation (Table 2). The ε can be derived using Eq. 6.

**Table 2** Two-parameters adsorption isotherm equations, isotherms constants and statistical comparison values for MB and MO on amidoxime PIM-1

| Isotherm | Equation* | Parameters | Dyes | | | | | |
|---|---|---|---|---|---|---|---|---|
| | | | Methylene Blue | | | Methyl Orange | | |
| | | | Temperature (K) | | | Temperature (K) | | |
| | | | 283 | 298 | 313 | 283 | 298 | 313 |
| Langmuir | $q_e = \frac{q_m K_L C_e}{1+K_L C_e}$ | $q_m$ (mg $g^{-1}$) | 86.0 | 79.3 | 73.7 | 92.9 | 88.1 | 79.2 |
| | | $K_L$ (L $mg^{-1}$) | 0.019 | 0.017 | 0.011 | 0.021 | 0.017 | 0.012 |
| | | $R_L$ | 0.10 | 0.10 | 0.15 | 0.09 | 0.10 | 0.14 |
| | | | 0.52 | 0.54 | 0.64 | 0.48 | 0.54 | 0.62 |
| | | SSE | 1.49 | 4.73 | 2.32 | 1.60 | 14.13 | 8.58 |
| | | $R^2$ | 0.999 | 0.997 | 0.998 | 0.999 | 0.993 | 0.993 |
| | | $\chi^2$ | 0.036 | 0.110 | 0.055 | 0.027 | 0.250 | 0.265 |
| | | Δq (%) | 1.51 | 2.35 | 1.96 | 1.08 | 3.08 | 4.83 |
| Freundlich | $q_e = K_F C_e^{1/n}$ | 1/n | 0.28 | 0.32 | 0.36 | 0.27 | 0.32 | 0.35 |
| | | $K_F$ (L $g^{-1}$) | 14.18 | 10.22 | 7.08 | 17.02 | 11.81 | 8.19 |
| | | SSE | 64.11 | 78.25 | 54.84 | 85.04 | 96.56 | 80.48 |
| | | $R^2$ | 0.953 | 0.958 | 0.952 | 0.947 | 0.955 | 0.941 |
| | | $\chi^2$ | 1.26 | 1.75 | 1.56 | 1.67 | 2.12 | 2.38 |
| | | Δq (%) | 8.38 | 9.73 | 11.58 | 9.53 | 10.10 | 14.40 |
| Temkin | $q_e = \left(\frac{RT}{b}\right)\ln(K_T C_e)$ | $K_T$ (L $g^{-1}$) | 0.25 | 0.19 | 0.11 | 0.30 | 0.19 | 0.11 |
| | | b (J $mol^{-1}$) | 147.75 | 151.80 | 152.84 | 139.84 | 136.55 | 142.43 |
| | | SSE | 19.68 | 19.06 | 12.50 | 29.42 | 31.09 | 23.24 |
| | | $R^2$ | 0.985 | 0.990 | 0.989 | 0.981 | 0.985 | 0.982 |
| | | $\chi^2$ | 0.32 | 0.34 | 0.27 | 0.52 | 0.64 | 0.59 |
| | | Δq (%) | 3.84 | 3.79 | 4.15 | 5.10 | 5.31 | 6.67 |
| D–R | $q_e = q_s \exp(-K_{DR}\varepsilon^2)$ | $q_s$ (mg $g^{-1}$) | 70.81 | 63.70 | 56.61 | 78.15 | 72.07 | 61.98 |
| | | $K_{DR}$ ($\times 10^{-4}$) ($mol^2$ $kJ^{-2}$) | 1.80 | 1.44 | 2.73 | 1.58 | 1.74 | 2.61 |
| | | SSE | 178.95 | 215.03 | 126.88 | 168.58 | 154.36 | 108.27 |
| | | $R^2$ | 0.879 | 0.893 | 0.895 | 0.900 | 0.930 | 0.922 |
| | | $\chi^2$ | 3.39 | 4.60 | 3.48 | 2.72 | 2.50 | 2.55 |
| | | Δq (%) | 13.04 | 14.66 | 16.38 | 10.79 | 9.33 | 13.20 |

*$q_m$ and $q_s$ are the equilibrium adsorption capacities of Langmuir and D–R isotherms, respectively. $C_e$ (mg $L^{-1}$) is the adsorbate concentration at the equilibrium. $K_L$, $K_F$, $K_T$, $K_{DR}$ are the equilibrium constants of respective isotherms. 1/n is the adsorption intensity, b is the heat of adsorption. R is the gas constant ($8.314 \times 10^{-3}$ kJ $K^{-1}$ $mol^{-1}$) and T is the absolute temperature (K) and ε is the Polanyi potential

**Table 3** Three-parameters adsorption isotherm equations, isotherms constants and statistical comparison values for MB and MO on amidoxime PIM-1

| Isotherm | Equation* | Parameters | Dyes | | | | | |
|---|---|---|---|---|---|---|---|---|
| | | | Methylene Blue | | | Methyl Orange | | |
| | | | Temperature (K) | | | Temperature (K) | | |
| | | | 283 | 298 | 313 | 283 | 298 | 313 |
| Redlich–Peterson | $q_e = \frac{q_m(K_R C_e)}{1+(K_R C_e)^{nR}}$ | $q_m$ (mg $g^{-1}$) | 86.11 | 78.29 | 73.73 | 92.16 | 85.45 | 79.25 |
| | | $K_R$ (L $mg^{-1}$) | 0.018 | 0.018 | 0.011 | 0.022 | 0.018 | 0.012 |
| | | $n_R$ | 1.00 | 0.99 | 1.00 | 1.00 | 0.99 | 1.00 |
| | | SSE | 1.50 | 4.63 | 2.32 | 1.59 | 13.97 | 8.58 |
| | | $R^2$ | 0.999 | 0.997 | 0.998 | 0.999 | 0.993 | 0.993 |
| | | $\chi^2$ | 0.036 | 0.106 | 0.055 | 0.027 | 0.258 | 0.265 |
| | | Δq (%) | 1.52 | 2.30 | 1.96 | 1.11 | 3.21 | 4.83 |
| Sips | $q_e = \frac{q_m K_S C_e^{ns}}{1+K_S C_e^{ns}}$ | $q_m$ (mg $g^{-1}$) | 87.00 | 81.29 | 73.71 | 92.95 | 88.07 | 79.25 |
| | | $K_S$ (L $mg^{-1}$) | 0.021 | 0.020 | 0.011 | 0.021 | 0.017 | 0.012 |
| | | ns | 0.961 | 0.945 | 1.000 | 1.000 | 1.000 | 1.000 |
| | | SSE | 1.16 | 4.23 | 2.32 | 1.60 | 14.13 | 8.58 |
| | | $R^2$ | 0.999 | 0.998 | 0.998 | 0.999 | 0.993 | 0.993 |
| | | $\chi^2$ | 0.022 | 0.093 | 0.055 | 0.027 | 0.250 | 0.265 |
| | | Δq (%) | 1.04 | 2.15 | 1.96 | 1.08 | 3.08 | 4.83 |
| Khan | $q_e = \frac{q_m K_K C_e}{(1+K_K C_e)^{nK}}$ | $q_m$ (mg $g^{-1}$) | 84.03 | 76.28 | 95.31 | 91.28 | 81.98 | 103.5 |
| | | $K_K$ (L $mg^{-1}$) | 0.019 | 0.018 | 0.008 | 0.022 | 0.019 | 0.009 |
| | | $n_K$ | 0.992 | 0.984 | 1.131 | 0.993 | 0.971 | 1.135 |
| | | SSE | 1.33 | 4.65 | 0.92 | 1.58 | 13.75 | 6.37 |
| | | $R^2$ | 0.999 | 0.997 | 0.999 | 0.999 | 0.993 | 0.995 |
| | | $\chi^2$ | 0.028 | 0.104 | 0.017 | 0.027 | 0.259 | 0.166 |
| | | Δq (%) | 1.24 | 2.26 | 0.91 | 1.12 | 3.25 | 3.58 |
| Liu | $q_e = \frac{q_m (K_{Liu} C_e)^{nLiu}}{1+(K_{Liu} C_e)^{nLiu}}$ | $q_m$ (mg $g^{-1}$) | 87.00 | 81.29 | 69.61 | 92.70 | 86.66 | 72.44 |
| | | $K_{Liu}$ (L $mg^{-1}$) | 0.018 | 0.016 | 0.013 | 0.021 | 0.018 | 0.015 |
| | | $n_{Liu}$ | 0.96 | 0.95 | 1.13 | 1.01 | 1.04 | 1.25 |
| | | SSE | 1.16 | 4.23 | 0.85 | 1.60 | 13.90 | 3.25 |
| | | $R^2$ | 0.999 | 0.998 | 0.999 | 0.999 | 0.993 | 0.997 |
| | | $\chi^2$ | 0.022 | 0.093 | 0.019 | 0.026 | 0.232 | 0.061 |
| | | Δq (%) | 1.04 | 2.15 | 1.08 | 1.04 | 2.87 | 1.82 |

*$q_m$ is the equilibrium adsorption capacity of respective isotherm. Ce (mg $L^{-1}$) is the adsorbate concentration at the equilibrium. $K_R$, $K_s$,$K_K$, $K_{Liu}$ are the equilibrium constants of respective isotherms. $n_R$, $n_s$, $n_K$ and $n_{Liu}$ are the model exponents of respective isotherms

$$\varepsilon = \mathrm{RTln}\left(1 + \frac{1}{C_e}\right) \quad (6)$$

where R is the gas constant ($8.314 \times 10^{-3}$ kJ $K^{-1}$ $mol^{-1}$) and T is the absolute temperature (K). $C_e$ is the equilibrium concentration which usually applied with the units of mg $L^{-1}$ or mol $L^{-1}$. However, Hu et al. [74], has shown that Polanyi potential calculated using $C_e$ is not correct since the logarithmic term must be dimensionless. The mean free energy (E) calculated by using ε value which is obtained by $C_e$ is incorrect. Therefore, we have avoided calculating the mean free energy from these values [74].

Considering three-parameter isotherm models, Redlich–Peterson and Sips isotherms are hybrid isotherms featuring both Langmuir and Freundlich isotherms. Their non-linear forms are presented in Table 3. These models combine three parameters into an empirical equation [68, 71]. Generally, minimizing procedure is applied to solve the equations by maximizing correlation coefficients between experimental and calculated values using Microsoft excel solver add-in function. Although numerous reports do not take into account, the values of exponents (n) ($n_R$ for Redlich–Peterson and ns; for Sips isotherm) should be $0 < n \leq 1$ in order to approximate correct parameters [61].

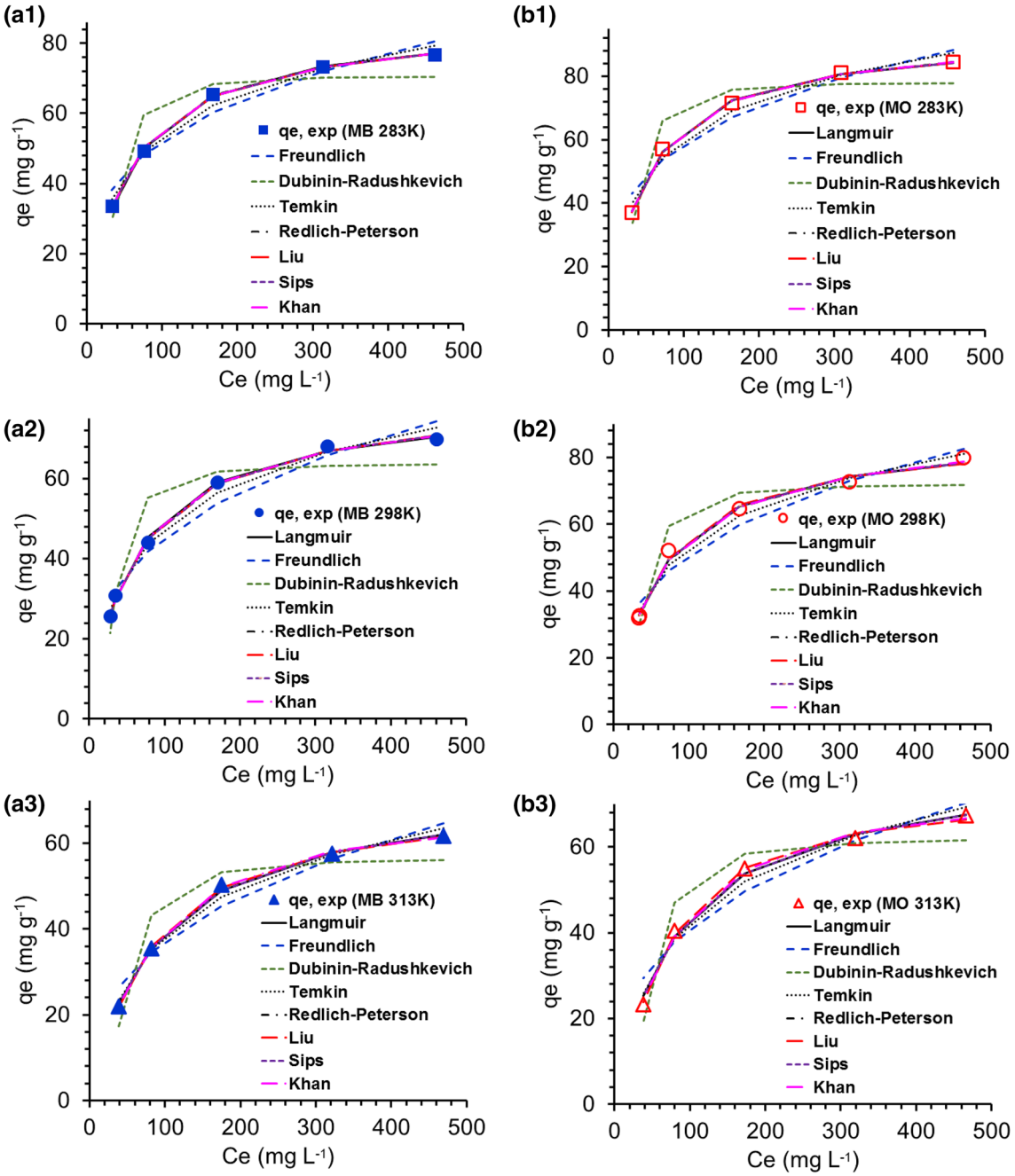


**Fig. 5** Comparison of adsorption isotherms for **a** MB and **b** MO adsorption on amidoxime PIM-1 at (1) 283 K, (2) 298 K and (3) 313 K

Khan isotherm is a generalized model proposed for the pure solutions and no restriction has been highlighted related to the values of isotherm parameters [70]. In addition, Liu isotherm is another isotherm model that combines Langmuir and Freundlich isotherm models [61, 71]. The monolayer assumption of Langmuir and the infinite adsorption assumption of Freundlich models are discarded by Liu model which assumes that the active sites of the adsorbent cannot possess the same energy. Furthermore, Liu model has no restriction regarding the exponent value ($n_{Liu}$) that could be any positive value unlike Redlich–Peterson and Sips isotherms exponents [61].

As it is demonstrated in Table 2, the best-fitted isotherm model considering the SSE, $R^2$, $\chi^2$ and $\Delta q$ values that obtained for two-parameter isotherms to be in the order of precision; Langmuir, Temkin, Freundlich and Dubinin–Radushkevich isotherms. Hence, the adsorption is better described by the Langmuir model, indicating both dyes adsorb as a

monolayer on the amidoxime PIM-1 surface. These results agree well with the previous studies performed by hydrolyzed and amine-modified PIM-1 samples [19, 20]. The feasibility of MB and MO adsorption onto amidoxime PIM-1 was further investigated using the dimensionless parameter of $R_L$ which is a derived parameter from the Langmuir equation as shown in Eq. 7.

$$R_L = \frac{1}{1 + K_L C_0} \tag{7}$$

where $C_0$ and $K_L$ are the initial concentration of dyes and the Langmuir constants for corresponding dyes. The adsorption can be described as reversible (0), favourable ($0 < R_L < 1$), unfavourable ($R_L > 1$) or linear ($R_L = 1$) depending on the $R_L$ values [75]. The $R_L$ values for adsorption of MB and MO on amidoxime PIM-1 are calculated between 0.10 and 0.64 (Table 2), revealing that the adsorption process is favourable. Furthermore, the relationship between $R_L$ values and temperature is presented in Table 2 which reveals that $R_L$ values increased with an increased temperature, indicating reduced temperature could promote the adsorption [60].

In general, three-parameter isotherm models have greater correlation coefficients ($R^2$) and lower relative errors ($\Delta q$) compared to two-parameter isotherms models. The experimental and calculated values are in good agreement for all three-parameter isotherm models. Hence, Liu and Khan isotherm models are provided the best correlations for the adsorption of both MB and MO on amidoxime PIM-1. Although mathematically correct, Khan isotherm model fails to predict correct equilibrium adsorption capacity ($q_m$) value at high temperature (313 K) as demonstrated in Table 3. Therefore, it was concluded that the adsorption of MB and MO on amidoxime PIM-1 was best described by Liu isotherm. In addition, the applicability of all isotherms indicates that both monolayer and heterogeneous surface conditions exist under the experimental conditions. Calculated $q_m$ values and isotherm parameters for all models are displayed in Table 3 for both MB and MO at various temperatures.

## Adsorption Thermodynamics

The thermodynamic parameters such as change in Gibbs free energy ($\Delta G^o$), change of enthalpy ($\Delta H^o$), and changes in entropy ($\Delta S^o$), express the feasibility of the adsorption process. The Van't Hoff equation (Eq. 8) has been commonly employed to determine those parameters by measuring the changes in the equilibrium constant with variations of temperatures [41, 76]. Hence, the equilibrium constant is the essential requirement to obtain correct values of thermodynamic parameters.

$$\Delta G^o = -RTlnK \tag{8}$$

where R, T and K represent the universal gas constant (8.314 J $K^{-1}$ $mol^{-1}$), the absolute temperature (K) and the thermodynamic equilibrium constant, respectively.

Regarding the 3rd principle of the thermodynamics;

$$\Delta G^o = \Delta H^o - T\Delta S^o \tag{9}$$

Combination of Eqs. 8 and 9 results in Eq. 10.

$$\ln K = -\frac{\Delta H^o}{RT} + \frac{\Delta S^o}{R} \tag{10}$$

Eventually, enthalpy ($\Delta H^o$) and entropy ($\Delta S^o$) values can be obtained by plotting ln K versus 1/T from the slope and the intercept of this graph, respectively. Although several different ways of using equilibrium constant can be found in adsorption literature [44–47], it is necessary to use correct equilibrium constant value to obtain correct thermodynamic values. The correct determination of equilibrium constant can be achieved by first obtaining adsorption isotherms at different temperatures and then making their non-linear fittings [41]. Furthermore, the equilibrium constants calculated from the adsorption isotherms are usually expressed in mg $L^{-1}$ or mol $L^{-1}$ which must be dimensionless to be used in Van't Hoff equation. Recently, Lima et al. [41] have reported the correct use of the equilibrium constant by using Eq. 11 which utilizes the equilibrium constants from the best-fitted isotherm and turns into dimensionless factor.

$$K = \frac{K_L \times 1000 \times \text{molecular weight of adsorbate}}{\gamma} \tag{11}$$

Based on the data from the adsorption of MB and MO on amidoxime PIM-1, Liu isotherm gave the best fit. Thus, Liu constants ($K_{Liu}$, L $mg^{-1}$) were calculated from the isotherms for each temperature (Table 3) to estimate thermodynamic parameters. Dimensionless equilibrium constants (K) were derived from Liu isotherm constants according to Eq. 11 [41] and presented in Table 4. Hence, thermodynamic parameters such as $\Delta G^o$ (gibbs free energy), $\Delta H^o$ (enthalpy) and $\Delta S^o$ (entropy) for the adsorption of MB and MO onto amidoxime PIM-1 were determined using Eqs. 8–10. ln K values were derived from dimensionless equilibrium constants (K) as provided in Table 4 and plots against 1/T (Fig. 6), which provides the values of $\Delta H°$ and $\Delta S°$ from the slope and intercept of graph based on the Eq. 10. The obtained values of $\Delta H°$ and $\Delta S°$ are also presented in Table 4. It can be seen that $\Delta H°$ has a negative value for both dyes (− 8.7 and − 9.3 kJ $mol^{-1}$ for MB and MO, respectively) suggesting the adsorption process is an exothermic process. This result is in line with the $R_L$ values obtained from Langmuir isotherm. On the other hand, $\Delta S°$ shows positive values for both dyes (41.6 and 40.7 J $K^{-1}$ $mol^{-1}$ for MB and MO, respectively) revealing increased randomness at the solid/solution interface. Consequently, $\Delta G^o$ values, were derived, which show

**Table 4** Calculated values of dimensionless equilibrium constants (K) based on Liu isotherm, enthalpy ($\Delta H^o$), entropy ($\Delta S^o$) and Gibb's free energy ($\Delta G^o$) values

| Isotherm | Parameters | Dyes | | | | | |
|---|---|---|---|---|---|---|---|
| | | Methylene Blue | | | Methyl Orange | | |
| | | Temperature (K) | | | Temperature (K) | | |
| | | 283 | 298 | 313 | 283 | 298 | 313 |
| Liu | ln K | 8.68 | 8.55 | 8.30 | 8.85 | 8.64 | 8.42 |
| | $\Delta H$ (kJ mol$^{-1}$) | | −8.7 | | | −9.3 | |
| | $\Delta S$ (J K$^{-1}$ mol$^{-1}$) | | 41.6 | | | 40.7 | |
| | $\Delta G$ (kJ mol$^{-1}$) | −20.46 | −21.08 | −21.70 | −20.86 | −21.47 | −22.08 |

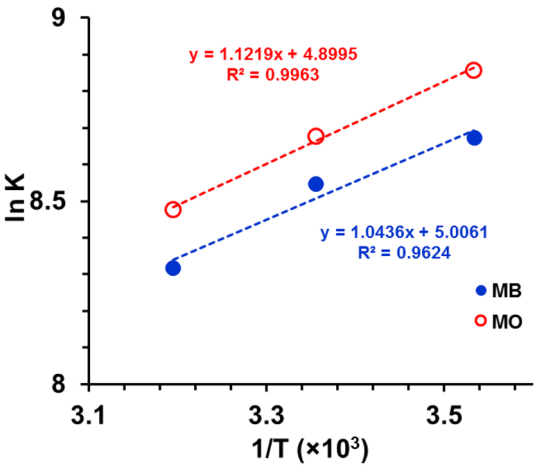


**Fig. 6** Plot of ln K versus 1/T for MB (filled circles) and MO (open circles) adsorption on amidoxime PIM-1

negative values (~(− 21 kJ mol$^{-1}$)) for all temperatures and both dyes, indicating the adsorption onto amidoxime PIM-1 is spontaneous and physical. Since the free energy change is less than 40 kJ mol$^{-1}$, adsorption considered as physical otherwise chemical adsorption presents.

## Desorption

Efficient desorption of dyes is also as important as the adsorption process since it indicates not only the reusability of the adsorbents but also the possible mechanism of the adsorption. When desorption occurs by only using water, it shows weakly attached adsorbate. If the desorption requires strong acid or base, it manifests that the attachment occurs by electrostatic interaction or ion exchange [77]. In our previous studies, we have presented that adsorbed dyes from modified PIM-1s could be desorbed simply using 1 M NaOH or 1 M HCl solutions in ethanol [31, 32] while treating with water does not help to desorb dyes from modified PIM-1s surface. Hence, amidoxime modified PIM-1s were first placed into neutral distilled water after the adsorption of MB and MO which showed no sign of desorption. This was further continued using a drop of 1 M HCl or 1 M NaOH solutions for MB and MO adsorbed amidoxime PIM-1s respectively. Although slight desorption was observed for both dyes, the complete desorption could not be obtained by using water. Therefore, we have placed dye–adsorbed amidoxime PIM-1 in ethanol solutions and 1 M HCl or 1 M NaOH solutions were added drop-wisely to these solutions. With the addition of acid or base, the solution became coloured with the desired species immediately as illustrated in Fig. S6 in supporting information, indicating the adsorption occurs by electrostatic attractions.

## Conclusions

Chemical modification of PIM-1 powder was achieved using hydroxylamine compound to obtain amidoxime PIM-1. Following the characterization of amidoxime PIM-1, dye uptake ability was investigated using MB and MO dyes from water. The non-linear regression analysis has been performed to analyze adsorption isotherm and kinetic models. Based on the data obtained from combined error analysis methods, Liu isotherm was found as the best isotherm model to describe the adsorption of both dyes on amidoxime PIM-1. The calculated equilibrium adsorption capacities ($q_m$) were found as 86.7 mg g$^{-1}$ and 81.3 mg g$^{-1}$ for MO and MB, respectively at pH 6 and 298 K. The calculated values were quite close to experimental values. Moreover, Amidoxime PIM-1 has the ability to adsorb both dyes from binary mixtures simultaneously. Furthermore, the affinity could be improved for the desired species by simply changing the pH of the solution. The pseudo-second-order kinetic model has the best fit for the adsorption. Thermodynamic parameters were determined by obtaining dimensionless equilibrium isotherms constants at various temperatures. Consequently, it was found that the adsorption of MB and MO onto amidoxime is physical, spontaneous and exothermic.

**Acknowledgements** The author would like to thank Prof. Aslihan Gunel for her technical help.

## References


1. Kurczewska J, Cegłowski M, Schroeder G (2019) Alginate/PAMAM dendrimer—halloysite beads for removal of cationic and anionic dyes. Int J Biol Macromol 123:398–408
2. Kale RD, Kane PB (2019) Colour removal of phthalocyanine based reactive dye by nanoparticles. Groundw Sustain Dev 8:309–318
3. Patra G, Barnwal R, Behera SK, Meikap BC (2018) Removal of dyes from aqueous solution by sorption with fly ash using a hydrocyclone. J Environ Chem Eng 6:5204–5211
4. Pandey N, Shukla SK, Singh NB (2017) Water purification by polymer nanocomposites: an overview. Nanocomposites 3:47–66
5. Kanmani P, Aravind J, Kamaraj M, Sureshbabu P, Karthikeyan S (2017) Environmental applications of chitosan and cellulosic biopolymers: a comprehensive outlook. Bioresour Technol 242:295–303
6. Reddy DHK, Lee SM (2013) Application of magnetic chitosan composites for the removal of toxic metal and dyes from aqueous solutions. Adv Colloid Interface Sci 201–202:68–93
7. Tan KB, Vakili M, Horri BA, Poh PE, Abdullah AZ, Salamatinia B (2015) Adsorption of dyes by nanomaterials: recent developments and adsorption mechanisms. Sep Purif Technol 150:229–242
8. Salleh MAM, Mahmoud DK, Karim WAWA, Idris A (2011) Cationic and anionic dye adsorption by agricultural solid wastes: a comprehensive review. Desalination 280:1–13
9. Demirbas A (2009) Agricultural based activated carbons for the removal of dyes from aqueous solutions: a review. J Hazard Mater 167:1–9
10. Banat IM, Nigam P, Singh D, Marchant R (1996) Microbial decolorization of textile-dye-containing effluents: a review. Bioresour Technol 58:217–227
11. Pearce CI, Lloyd JR, Guthrie JT (2003) The removal of colour from textile wastewater using whole bacterial cells: a review. Dyes Pigm 58:179–196
12. Lau WJ, Ismail AF (2009) Polymeric nanofiltration membranes for textile dye wastewater treatment: preparation, performance evaluation, transport modelling, and fouling control—a review. Desalination 245:321–348
13. Ali H (2010) Biodegradation of synthetic dyes—a review. Water Air Soil Pollut 213:251–273
14. Verma AK, Dash RR, Bhunia P (2012) A review on chemical coagulation/flocculation technologies for removal of colour from textile wastewaters. J Environ Manag 93:154–168
15. Oller I, Malato S, Sánchez-Pérez JA (2011) Combination of advanced oxidation processes and biological treatments for wastewater decontamination—a review. Sci Total Environ 409:4141–4166
16. Ahmad A, Mohd-Setapar SH, Chuong CS, Khatoon A, Wani WA, Kumar R, Rafatullah M (2015) Recent advances in new generation dye removal technologies: novel search for approaches to reprocess wastewater. RSC Adv 5:30801–30818
17. Singh NB, Nagpal G, Agrawal S (2018) Rachna, water purification by using adsorbents: a review. Environ Technol Innov 11:187–240
18. Kyzas GZ, Bikiaris DN, Mitropoulos AC (2017) Chitosan adsorbents for dye removal: a review. Polym Int 66:1800–1811
19. Sun L, Chen D, Wan S, Yu Z (2018) Adsorption studies of dimetridazole and metronidazole onto biochar derived from sugarcane bagasse: kinetic, equilibrium, and mechanisms. J Polym Environ 26:765–777
20. Murugesan A, Divakaran M, Raveendran P, Nitin Nikamanth AB, Thelly KJ (2019) An eco-friendly porous poly(imide-ether)s for the efficient removal of methylene blue: adsorption kinetics, isotherm, thermodynamics and reuse performances. J Polym Environ 27:1007–1024
21. Budd PM, Ghanem BS, Makhseed S, McKeown NB, Msayib KJ, Tattershall CE (2004) Polymers of intrinsic microporosity (PIMs): robust, solution-processable, organic nanoporous materials. Chem Commun. https://doi.org/10.1039/B311764B
22. McKeown NB, Budd PM, Msayib KJ, Ghanem BS, Kingston HJ, Tattershall CE, Makhseed S, Reynolds KJ, Fritsch D (2005) Polymers of intrinsic microporosity (PIMs): bridging the void between microporous and polymeric materials. Chem-Eur J 11:2610–2620
23. Satilmis B, Budd PM (2017) Selective dye adsorption by chemically-modified and thermally-treated polymers of intrinsic microporosity. J Colloid Interface Sci 492:81–91
24. Tsarkov S, Khotimskiy V, Budd PM, Volkov V, Kukushkina J, Volkov A (2012) Solvent nanofiltration through high permeability glassy polymers: effect of polymer and solute nature. J Membr Sci 423–424:65–72
25. Satilmis B, Uyar T (2018) Removal of aniline from air and water by polymers of intrinsic microporosity (PIM-1) electrospun ultrafine fibers. J Colloid Interface Sci 516:317–324
26. Pan Y, Zhang LJ, Li ZJ, Ma LJ, Zhang YF, Wang J, Meng JQ (2018) Hierarchical porous membrane via electrospinning PIM-1 for micropollutants removal. Appl Surf Sci 443:441–451
27. Zhang CL, Li P, Cao B (2016) Electrospun polymer of intrinsic microporosity fibers and their use in the adsorption of contaminants from a nonaqueous system. J Appl Polym Sci. https://doi.org/10.1002/app.43475
28. Wu XM, Zhang QG, Soyekwo F, Liu QL, Zhu AM (2016) Pervaporation removal of volatile organic compounds from aqueous solutions using the highly permeable PIM-1 membrane. AlChE J 62:842–851
29. Satilmis B, Budd PM (2014) Base-catalysed hydrolysis of PIM-1: amide versus carboxylate formation. RSC Adv 4:52189–52198
30. Satilmis B, Alnajrani MN, Budd PM (2015) Hydroxyalkylaminoalkylamide PIMs: selective adsorption by ethanolamine- and diethanolamine-modified PIM-1. Macromolecules 48:5663–5669
31. Satilmis B, Uyar T (2018) Amine modified electrospun PIM-1 ultrafine fibers for an efficient removal of methyl orange from an aqueous system. Appl Surf Sci 453:220–229
32. Satilmis B, Budd PM, Uyar T (2017) Systematic hydrolysis of PIM-1 and electrospinning of hydrolyzed PIM-1 ultrafine fibers for an efficient removal of dye from water. React Funct Polym 121:67–75
33. Ramakrishna S, Fujihara K, Teo W-E, Lim T-C, Ma Z (2005) An introduction to electrospinning and nanofibers. World Scientific
34. Bhardwaj N, Kundu SC (2010) Electrospinning: a fascinating fiber fabrication technique. Biotechnol Adv 28:325–347
35. Satilmis B, Isık T, Demir MM, Uyar T (2019) Amidoxime functionalized polymers of intrinsic microporosity (PIM-1) electrospun ultrafine fibers for rapid removal of uranyl ions from water. Appl Surf Sci 467–468:648–657
36. Sihn YH, Byun J, Patel HA, Lee W, Yavuz CT (2016) Rapid extraction of uranium ions from seawater using novel porous polymeric adsorbents. RSC Adv 6:45968–45976
37. Patel HA, Yavuz CT (2012) Noninvasive functionalization of polymers of intrinsic microporosity for enhanced $CO_2$ capture. Chem Commun 48:9989–9991
38. Abels C, Carstensen F, Wessling M (2013) Membrane processes in biorefinery applications. J Membr Sci 444:285–317
39. Ren Q, Xing H, Bao Z, Su B, Yang Q, Yang Y, Zhang Z (2013) Recent advances in separation of bioactive natural products. Chin J Chem Eng 21:937–952
40. Topuz F, Satilmis B, Uyar T (2019) Electrospinning of uniform nanofibers of Polymers of Intrinsic Microporosity (PIM-1): the

influence of solution conductivity and relative humidity. Polymer 178:121610
41. Lima EC, Hosseini-Bandegharaei A, Moreno-Piraján JC, Anastopoulos I (2019) A critical review of the estimation of the thermodynamic parameters on adsorption equilibria. Wrong use of equilibrium constant in the Van't Hoof equation for calculation of thermodynamic parameters of adsorption. J Mol Liq 273:425–434
42. Foo KY, Hameed BH (2010) Insights into the modeling of adsorption isotherm systems. Chem Eng J 156:2–10
43. Günay A, Arslankaya E, Tosun İ (2007) Lead removal from aqueous solution by natural and pretreated clinoptilolite: adsorption equilibrium and kinetics. J Hazard Mater 146:362–371
44. Budd PM, Msayib KJ, Tattershall CE, Ghanem BS, Reynolds KJ, McKeown NB, Fritsch D (2005) Gas separation membranes from polymers of intrinsic microporosity. J Membr Sci 251:263–269
45. Budd PM, McKeown NB, Fritsch D (2006) Polymers of intrinsic microporosity (PIMs): high free volume polymers for membrane applications. Macromol Symp 245:403–405
46. Vopicka O, Friess K, Hynek V, Sysel P, Zgazar M, Sipek M, Pilnacek K, Lanc M, Jansen JC, Mason CR, Budd PM (2013) Equilibrium and transient sorption of vapours and gases in the polymer of intrinsic microporosity PIM-1. J Membr Sci 434:148–160
47. Anokhina TS, Yushkin AA, Budd PM, Volkov AV (2015) Application of PIM-1 for solvent swing adsorption and solvent recovery by nanofiltration. Sep Purif Technol 156:683–690
48. Wang Y, McKeown NB, Msayib KJ, Turnbull GA, Samuel IDW (2011) Laser chemosensor with rapid responsivity and inherent memory based on a polymer of intrinsic microporosity. Sensors (Basel, Switzerland) 11:2478–2487
49. Short R, Carta M, Bezzu CG, Fritsch D, Kariuki BM, McKeown NB (2011) Hexaphenylbenzene-based polymers of intrinsic microporosity. Chem Commun 47:6822–6824
50. Mackintosh HJ, Budd PM, McKeown NB (2008) Catalysis by microporous phthalocyanine and porphyrin network polymers. J Mater Chem 18:573–578
51. Xia FJ, Pan M, Mu SC, Malpass-Evans R, Carta M, McKeown NB, Attard GA, Brew A, Morgan DJ, Marken F (2014) Polymers of intrinsic microporosity in electrocatalysis: novel pore rigidity effects and lamella palladium growth. Electrochim Acta 128:3–9
52. Ma H, Kong A, Ji Y, He B, Song Y, Li J (2019) Ultrahigh adsorption capacities for anionic and cationic dyes from wastewater using only chitosan. J Clean Prod 214:89–94
53. Igberase E, Ofomaja A, Osifo PO (2019) Enhanced heavy metal ions adsorption by 4-aminobenzoic acid grafted on chitosan/epichlorohydrin composite: kinetics, isotherms, thermodynamics and desorption studies. Int J Biol Macromol 123:664–676
54. Harrache Z, Abbas M, Aksil T, Trari M (2019) Thermodynamic and kinetics studies on adsorption of Indigo Carmine from aqueous solution by activated carbon. Microchem J 144:180–189
55. Lagergren S (1898) Zur theorie der sogenannten adsorption geloster stoffe, Handlingar, 24, Kungliga svenska vetenskapsakademiens. Band 24:1–39
56. Ho YS, McKay G (1999) Pseudo-second-order model for sorption processes. Process Biochem 34:451–465
57. McLintock IS (1967) The Elovich Equation in chemisorption kinetics. Nature 216:1204–1205
58. Weber WJ, Morris JC (1963) Kinetics of adsorption on carbon from solution. J Sanit Eng Div 89:31–60
59. Khan EA, Shahjahan TA, Khan TA (2018) Adsorption of methyl red on activated carbon derived from custard apple (*Annona squamosa*) fruit shell: equilibrium isotherm and kinetic studies. J Mol Liq 249:1195–1211
60. Liu Y, Liu X, Dong W, Zhang L, Kong Q, Wang W (2017) Efficient adsorption of sulfamethazine onto modified activated carbon: a plausible adsorption mechanism. Sci Rep 7:12437
61. Lima ÉC, Adebayo MA, Machado FM (2015) Carbon nanomaterials as adsorbents for environmental and biological applications. Brazil
62. Özcan A, Öncü EM, Özcan AS (2006) Adsorption of Acid Blue 193 from aqueous solutions onto DEDMA-sepiolite. J Hazard Mater 129:244–252
63. Ahmadi M, Mohammadian M, Khosravi-Nikou MR, Baghban A (2019) Experimental, kinetic, and thermodynamic studies of adsorptive desulfurization and denitrogenation of model fuels using novel mesoporous materials. J Hazard Mater 374:129–139
64. Langmuir I (1916) The Constitution and fundamental properties of solids and liquids. Part I solids. J Am Chem Soc 38:2221–2295
65. Freundlich HMF (1906) Over the adsorption in solution. J Phys Chem 57:385–471
66. Tempkin MI, Pyzhev V (1940) Kinetics of ammonia synthesis on promoted iron catalyst. Acta Phys Chim USSR 12:327–356
67. Dubinin MM, Radushkevich LV (1947) The equation of the characteristic curve of activated charcoal. Proc Acad Sci USSR Phys Chem Sect 55:331–337
68. Redlich O, Peterson DL (1959) A useful adsorption isotherm. J Phys Chem 63:1024–1024
69. Sips R (1948) On the structure of a catalyst surface. J Chem Phys 16:490–495
70. Khan AR, Ataullah R, Al-Haddad A (1997) Equilibrium adsorption studies of some aromatic pollutants from dilute aqueous solutions on activated carbon at different temperatures. J Colloid Interface Sci 194:154–165
71. Liu Y, Xu H, Yang S-F, Tay J-H (2003) A general model for biosorption of $Cd^{2+}$, $Cu^{2+}$ and $Zn^{2+}$ by aerobic granules. J Biotechnol 102:233–239
72. Vijayaraghavan K, Padmesh TVN, Palanivelu K, Velan M (2006) Biosorption of nickel(II) ions onto Sargassum wightii: application of two-parameter and three-parameter isotherm models. J Hazard Mater 133:304–308
73. Dubinin MM (1960) The potential theory of adsorption of gases and vapors for adsorbents with energetically nonuniform surfaces. Chem Rev 60:235–241
74. Hu Q, Zhang Z (2019) Application of Dubinin-Radushkevich isotherm model at the solid/solution interface: a theoretical analysis. J Mol Liq 277:646–648
75. Ada K, Ergene A, Tan S, Yalçın E (2009) Adsorption of Remazol Brilliant Blue R using ZnO fine powder: equilibrium, kinetic and thermodynamic modeling studies. J Hazard Mater 165:637–644
76. Ghosal PS, Gupta AK (2017) Determination of thermodynamic parameters from Langmuir isotherm constant-revisited. J Mol Liq 225:137–146
77. Fu J, Zhu J, Wang Z, Wang Y, Wang S, Yan R, Xu Q (2019) Highly-efficient and selective adsorption of anionic dyes onto hollow polymer microcapsules having a high surface-density of amino groups: Isotherms, kinetics, thermodynamics and mechanism. J Colloid Interface Sci 542:123–135